Computational and Theoretical Chemistry 1175 (2020) 112711

Contents lists available at ScienceDirect

Computational and Theoretical Chemistry

journal homepage: www.elsevier.com/locate/comptc

Real-space quasi-relativistic quantum chemistry

Joel Anderson[a,*], Robert J. Harrison[a], Bryan Sundahl[a], W. Scott Thornton[a], Gregory Beylkin[b]

[a] Institute for Advanced Computational Science, Stony Brook University, Stony Brook, NY 11794-5250, United States
[b] Department of Applied Mathematics, University of Colorado at Boulder, UCB 526, Boulder, CO 80309-0526, United States

ARTICLE INFO

Keywords:
Quasi-relativistic
Douglas-Kroll
Electronic structure
Multiresolution analysis
Quantum chemistry

ABSTRACT

We present for the first time real-space, arbitrarily-accurate representations of the operators required for up to second-order Douglas-Kroll-Hess (DKH), a model for constructing quasi-relativistic electronic Hamiltonians. The approach can be extended to other operator-based quasi-relativistic models. The representations are in the form of sums of Gaussian functions with positive coefficients and thus enable efficient and numerically-accurate formulations using conventional Gaussian basis sets or other bases such as multiwavelets. The operators are demonstrated with application to hydrogen-like systems using the relativistic-kinematic and first-order DKH Hamiltonians.

1. Introduction

Accounting for the effects of special relativity is required to achieve high accuracy for all elements across the periodic table, and even qualitative accuracy for heavier elements [1]. The difficulty in doing so comes in finding an efficient and stable way to solve the Dirac equation, where solutions are 4-component complex-valued functions. Due to the nature of the spectrum of the Dirac Hamiltonian, a common approach is to decouple the equations into a 2-component formalism that solves only for the electronic (positive energy) states [2–5]. However, the operators necessary in this decoupling are typically formulated in momentum space, while most practical computations employ real-space numerical methods. Our motivation for finding real-space representations of the operators involved in these decoupling formalisms came from the development of relativistic quantum chemical methods using multiwavelet bases [6], where the common approach [7] of using matrix projections cannot be used. Specifically, the large size of multiwavelet bases (typically thousands of functions per electron compared with tens per electron for mainstream atom-centered bases) makes forming and manipulating matrix representations of operators prohibitive for practical calculations, and motivates us to use an approximately-decoupled operator with an explicit real-space representation. It is for this reason that we have developed arbitrarily-accurate representations of the operators required for up to second-order Douglass-Kroll-Hess (DKH), a model for constructing quasi-relativistic Hamiltonians [2,7]. The approach can be extended to other operator-based quasi-relativistic models. The new real-space representation of the operators are also relevant to mainstream atom-centered basis sets that typically employ Gaussian expansions for radial components by eliminating one source of basis set incompleteness — this is discussed further below.

We give a brief introduction into 2-component methods in Section 1.1 and the steps necessary to extend this approach in the multiwavelet basis in Section 1.2. Because of the properties of the basis set used, the DKH decoupling scheme is the focus of this paper, and thus most attention is given to the DKH formalism in Section 1.1, with only a brief mention of other methods.

1.1. 2-Component Theory

We review the 4-component Dirac Hamiltonian and describe current approaches to its decoupling. We only state formulas that will be used later in the paper. For more detailed descriptions of the various 2-component methods, see the original papers in [2–5] and reviews in [8–10].

The relativistic single-particle Dirac-Coulomb Hamiltonian is given by

$$h_d = c\boldsymbol{\alpha}\cdot\mathbf{p} + \beta mc^2 + V, \tag{1}$$

where c is the speed of light in atomic units, $\mathbf{p}$ is the 3-component vector of linear momentum operators $p_i = -i\hbar\frac{\partial}{\partial x_i}$, $V = -Z/r$ is the nuclear potential function for a single atom (as will be the case for all calculations in this work, though many-nucleus systems are possible), and the matrices α_1, α_2, α_3, and β are defined by the standard representation as

* Corresponding author.
E-mail address: joel.s.anderson@stonybrook.edu (J. Anderson).

https://doi.org/10.1016/j.comptc.2020.112711
Received 30 October 2019; Received in revised form 9 January 2020; Accepted 10 January 2020
Available online 17 January 2020
2210-271X/

$$\alpha_k = \begin{bmatrix} 0 & \sigma_k \\ \sigma_k & 0 \end{bmatrix}, \text{ and } \beta = \begin{bmatrix} I_2 & 0 \\ 0 & -I_2 \end{bmatrix}, \tag{2}$$

where

$$\sigma_1 = \begin{bmatrix} 0 & 1 \\ 1 & 0 \end{bmatrix}, \quad \sigma_2 = \begin{bmatrix} 0 & i \\ -i & 0 \end{bmatrix}, \quad \sigma_3 = \begin{bmatrix} 1 & 0 \\ 0 & -1 \end{bmatrix}. \tag{3}$$

The four-component eigenfunctions ψ of the Dirac Hamiltonian are often written as

$$\psi = \begin{bmatrix} \psi_L \\ \psi_S \end{bmatrix}, \tag{4}$$

where ψ_L and ψ_S are the "large" and the "small" components. The components are named for the fact that, when considering positive-energy states, the norm of the former outstrips the norm of the latter by a factor of approximately c. These solutions are of interest in chemistry because positive energy states correspond to possible electronic states, whereas negative energy states describe positrons. This motivates the decoupling of the equation in order to form a 2-component system that can fully describe the electronic states.

Decoupling of the one-electron Dirac Hamiltonian is achieved in a variety of ways. A recent popular approach due to Kutzelnigg and Liu [5] works directly with the matrix form of the operator to numerically decouple the different states within the chosen basis to numerical precision. This built upon similar approaches from Dyall [11,12] and Barysz and Sadlej [3] that instead start with the matrix projection of a transformed Hamiltonian. Predating these are methods which form matrices from an approximately-decoupled operator [13,2] (with no numerical decoupling step), such as the DKH method.

The DKH decoupling applies a series of unitary transformations to the Dirac Hamiltonian that successively reduce the order of the off-diagonal blocks in powers of V. The first of these transformations is necessarily the free-particle Foldy-Wouthuysen transformation, resulting in the first-order DKH Hamiltonian (DKH1), given by

$$U_0 h_d U_0^\dagger = \begin{bmatrix} E_o(p) - mc^2 + \mathcal{V} & O_1(p) \\ -O_1(p) & -E_0(p) - mc^2 + \mathcal{V} \end{bmatrix} \tag{5}$$

$$\mathcal{V} = A(V + \overline{P}(\boldsymbol{\sigma}\cdot\mathbf{p})V\overline{P}(\boldsymbol{\sigma}\cdot\mathbf{p}))A \tag{6}$$

$$h_{DKH1} = E_0(p) - mc^2 + \mathcal{V} = E_0(p) - mc^2 + A(V + \overline{P}(\boldsymbol{\sigma}\cdot\mathbf{p})V\overline{P}(\boldsymbol{\sigma}\cdot\mathbf{p}))A, \tag{7}$$

where $\boldsymbol{\sigma}$ is the vector of σ matrices, and with the following operators

$$E_0(p) = \sqrt{p^2c^2 + m^2c^4}, \tag{8}$$

$$\overline{P}(p) = c(E_0(p) + mc^2)^{-1}, \tag{9}$$

$$A(p) = \sqrt{\frac{E_0(p) + mc^2}{2E_0(p)}}, \tag{10}$$

and

$$O_1(p) = A\overline{P}(\boldsymbol{\sigma}\cdot\mathbf{p})VA - AV\overline{P}(\boldsymbol{\sigma}\cdot\mathbf{p})A \tag{11}$$

with $p = \sqrt{\|\mathbf{p}\|^2}$.

In (5) the rest energy term mc^2 has been subtracted from the diagonal so that the resulting energies can be more readily compared to their non-relativistic counterparts. The off-diagonal term O_1, represents the remaining coupling between the large and small components, and is neglected in the first-order DKH scheme. The second transformation, leading to the DKH2 Hamiltonian, eliminates O_1, generating the next block-diagonal terms as well as O_2, an off-diagonal block that is second-order in the potential. The details of the derivation can be found in [7]. The resulting Hamiltonian is given by:

$$h_{DKH2} = h_{DKH1} + \frac{1}{2}(W_1O_1 + O_1W_1), \tag{12}$$

with integral operator W_1:

$$W_1\left(\mathbf{p}, \mathbf{p}'\right) = \frac{A\overline{P}(\boldsymbol{\sigma}\cdot\mathbf{p})V(\mathbf{p}, \mathbf{p}')A - AV(\mathbf{p}, \mathbf{p}')\overline{P}(\boldsymbol{\sigma}\cdot\mathbf{p})A}{E_0(\mathbf{p}) + E_0(\mathbf{p}')}. \tag{13}$$

where we note that the nuclear potential is also an integral operator in momentum space.

A final operator to consider is the so-called "relativistic kinematics" Hamiltonian given by

$$h_{RK} = E_0 - mc^2 + V. \tag{14}$$

Although this Hamiltonian is not sufficiently accurate for quantum chemical calculations, it is used in this paper to aid in verification.

One may notice that the operators described above are expressed as functions of momentum, whereas most quantum chemical calculations use real-space basis functions (typically atom-centered linear combinations or contractions of Gaussian functions). The common approach, first described by Hess [7] is to diagonalize the selected uncontracted basis to form approximate eigenfunctions of the p^2 operator. Matrix elements in the basis of these approximate eigenfunctions have simple expressions, and the solution of the resulting matrix equations can be transformed back to give a representation in the original basis. Van Wüllen [14] identifies three sources of error in this approach: the basis set truncation error, error in the resolution of the identity from transformation of the basis set (for second- and higher-order DKH Hamiltonians), and error in computing with a basis set of approximate eigenfunctions of p^2. The diagonalization of the uncontracted basis set under p^2 suffers from ill-conditioning due to the exceptionally wide range in the magnitudes of exponents used in Gaussian basis sets for heavy atoms. The approach in this paper looks to alleviate the momentum space error and sidestep the ill-conditioned diagonalization by giving a method of applying these operators in real-space. This is accomplished in Section 2.

1.2. Integral equation approach for application in the multiresolution basis

Details of multiresolution multiwavelet bases and their application to quantum chemistry calculations can be found in [15,16] and references therein. Briefly, wavefunctions are represented in an adaptively-refined basis set of piecewise Legendre polynomials. The discontinuous nature of the basis functions and the number of coefficients in said basis make traditional matrix operator approaches intractable. Additionally, in this basis the application of the kinetic energy operator is ill-conditioned. Consequently, the integral form of the equations, rather than the differential form, is solved. Rearrangement of the DKH1 eigenvalue equation yields, for eigenfunction ψ and eigenvalue ϵ,

$$(E_0(p) - mc^2 - \epsilon)\psi = -A(V + \overline{P}(\boldsymbol{\alpha}\cdot\mathbf{p})V\overline{P}(\boldsymbol{\alpha}\cdot\mathbf{p}))\psi. \tag{15}$$

We solve this equation by first constructing the inverse of the operator on the left. Defining it as $\overline{E}$,

$$\overline{E}(p, \varepsilon = \epsilon) = \frac{1}{E_0(p) - mc^2 - \epsilon}, \tag{16}$$

we construct its representation in real space as well.

Application of the operator in (16) to both sides of (15) yields an equation that we solve by fixed-point iteration to obtain the eigenfunction.

$$\psi_{i+1} = -\overline{E}(p, \epsilon_i)(A(V + \overline{P}(\boldsymbol{\alpha}\cdot\mathbf{p})V\overline{P}(\boldsymbol{\alpha}\cdot\mathbf{p}))\psi_i) \tag{17}$$

At each iteration i, an estimate for the energy is calculated using

$$\epsilon_i = \frac{\langle\psi_i|h_{DKH1}|\psi_i\rangle}{\langle\psi_i|\psi_i\rangle}. \tag{18}$$

Application of E_0 in (18) is achieved by first applying the non-relativistic kinetic energy operator, and then applying a correction operator,

$$E_0(p)\psi = \frac{\sqrt{p^2c^2 + m^2c^4} - mc^2}{\frac{1}{2}p^2}\frac{1}{2}p^2\psi = \overline{T}(p)\frac{1}{2}p^2\psi, \tag{19}$$

where the operator $\overline{T}$ is defined as

$$\overline{T}(p) = \frac{\sqrt{p^2c^2 + m^2c^4} - mc^2}{\frac{1}{2}p^2} = \frac{2mc^2}{E_0 + mc^2}. \tag{20}$$

Thus to compute in multiwavelet bases, the two additional operators $\overline{E}$ and $\overline{T}$ are required as well as those normally prescribed by Eq. (7).

Note that all of these momentum-space operators are smooth at the origin (their first derivatives vanish there) and for large p decay to their asymptotic values as $O(p^{-1})$, and hence we can anticipate that their real-space representations will behave as $O(r^{-2})$ near the origin and will decay exponentially at long range. In prior work [15,17,18,6], we have developed several approaches to construct accurate and efficient representations of such functions (notably Green's functions of physically-relevant operators) as linear combinations of exponentials or Gaussians. Such representations have made practical the use of multiwavelet bases for simulation of electronic [6] and nuclear systems [19], and are also used in other real-space codes [20].

2. Derivation of representations

Our goal is to represent relativistic integral operators via a linear combination of Gaussian convolution operators with as few terms as possible with controlled accuracy, similar to the approach in e.g. [6,18,21]. The relativistic operators are defined in momentum space as multiplication operators by a radial function and, using appropriate identities, we construct their integral representations via Gaussians. We then proceed to either (i) discretize integral representations in momentum space to obtain a linear combination of Gaussians and then use the Fourier transform to obtain Gaussian convolutions in the real space or (ii) analytically transform integral identities into real space and discretize them after such transformation. While it may appear that these steps should commute, we note that the ranges of validity and the behavior of the error (other than the L^2-norm error) differ under the Fourier transform and, therefore, the resulting expansions depend on the chosen order of steps.

We consider four relativistic operators given in (20), (10), (16), and

$$\overline{P}(p)A(p) = c(E_0(p) + mc^2)^{-1}\sqrt{\frac{E_0(p) + mc^2}{2E_0(p)}}. \tag{21}$$

We note that $\overline{P}$ (Eq. (9)) only differs from $\overline{T}$ (Eq. (20)) by multiplication by a scalar.

2.1. Relevant identities and forms

We use two integral identities in order to generate the Gaussian expansion of the operator kernels,

$$x^{-\alpha} = \frac{1}{\Gamma(\alpha/2)}\int_{-\infty}^{\infty}\exp(-x^2\exp(-t) - \alpha t/2))dt \text{ for } \alpha > 0 \tag{22}$$

$$x^{-1} = \int_0^{\infty}\exp\Big(-xs\Big)ds = \int_{-\infty}^{\infty}\exp\Big(-x\exp(t) + t\Big)dt \tag{23}$$

and

$$\exp\Big(-xy\Big) = \frac{x}{2\sqrt{\pi}}\int_{-\infty}^{\infty}\exp(-x^2\exp(t)/4 - y^2\exp(-t) + t/2)dt, \tag{24}$$

(see [18] for the derivation details and for proof that the approximations based upon numerical quadrature of (24) maintain uniform relative error as stated in (89).

We also recall that the 3D Fourier transform of a spherically symmetric function $f(r)$ (with $r = \|\mathbf{r}\|$ and $p = \|\mathbf{p}\|$) is given by

$$F(p) = \frac{4\pi}{p}\int_0^{\infty} f(r)\sin(pr)rdr \tag{25}$$

and the inverse Fourier transform by

$$f(r) = \frac{1}{2\pi^2 r}\int_0^{\infty} F(p)\sin(pr)pdp, \tag{26}$$

where the Fourier transform is defined as

$$F(\mathbf{p}) = \int_{\mathbb{R}^3} f(\|\mathbf{r}\|)e^{-i\mathbf{r}\cdot\mathbf{p}}d\mathbf{r}. \tag{27}$$

2.2. Representation of operator $\overline{T}$

Theorem 1. *Operator $\overline{T}$ has an integral representation*

$$\overline{T}(p) = \int_{-\infty}^{\infty} e^{-\|\mathbf{p}\|^2 e^{-t}} w(t, mc)dt, \tag{28}$$

with the weight

$$w(t, mc) = \frac{2mc}{\sqrt{\pi}}e^{-\frac{1}{2}t}e^{-m^2c^2e^{-t}} - 2m^2c^2e^{-t}\text{erfc}(mce^{-t/2}), \tag{29}$$

where $w\Big(t - \tau, mce^{-\frac{1}{2}\tau}\Big) = w(t, mc)$ *or* $w(t, mc) = w(t - 2\log(mc), 1)$. *Spatial representation of $\overline{T}$ is then*

$$\overline{T}(r) = \int_{-\infty}^{\infty} e^{-\frac{1}{4}e^t r^2}\left(\frac{a}{\sqrt{2\pi}}e^{-a^2e^{-t}+t} - \frac{a^2}{\sqrt{2}}e^{\frac{1}{2}t}\text{erfc}(ae^{-t/2})\right)dt, \tag{30}$$

where $a = mc$.

Proof. We have

$$\overline{T}(p) = 2mc^2(E_0(p) + mc^2)^{-1} = \frac{2mc^2}{\sqrt{p^2c^2 + m^2c^4} + mc^2} = \frac{2a}{\sqrt{p^2 + a^2} + a}, \tag{31}$$

where $a = mc$. Combining integral identities

$$\frac{2a}{\sqrt{p^2 + a^2} + a} = 2a\int_0^{\infty} e^{-s(\sqrt{p^2+a^2}+a)}ds \tag{32}$$

and

$$e^{-s\sqrt{p^2+a^2}} = \frac{s}{2\sqrt{\pi}}\int_{-\infty}^{\infty} e^{-s^2e^t/4-(p^2+a^2)e^{-t}+\frac{1}{2}t}dt, \tag{33}$$

obtained from (24), where we set $x = s$ and $y = \sqrt{p^2 + a^2}$, we obtain

$$\frac{2a}{\sqrt{p^2 + a^2} + a} = 2a\int_{-\infty}^{\infty}\left(\int_0^{\infty}\frac{s}{2\sqrt{\pi}}e^{-s^2e^t/4}e^{-as}ds\right)e^{-(p^2+a^2)e^{-t}+\frac{1}{2}t}dt. \tag{34}$$

Since

$$\int_0^{\infty}\frac{s}{2\sqrt{\pi}}e^{-s^2e^t/4}e^{-as}ds = \frac{1}{\sqrt{\pi}}e^{-t} - ae^{a^2e^{-t}-\frac{3}{2}t}\text{erfc}(ae^{-t/2}), \tag{35}$$

where

$$\text{erfc}(z) = 1 - \text{erf(z)} = 1 - \frac{2}{\sqrt{\pi}}\int_0^z e^{-t^2}dt, \tag{36}$$

is the complimentary error function, we obtain (28) and (29). The weight $w(t, 1)$ is illustrated in Fig. 1. Computing the Fourier transform

$$\frac{1}{(2\pi)^{3/2}}\int_{\mathbb{R}^3} e^{-p^2e^{-t}}e^{i\mathbf{r}\mathbf{p}}d\mathbf{p} = \frac{1}{2^{3/2}}e^{\frac{3}{2}t-\frac{1}{4}e^t r^2}, \tag{37}$$

we obtain spatial representation of $\overline{T}$ in (30). □

Discretizing this integral and applying the inverse Fourier transform to the result, we obtain a spatial representation of the operator $\overline{T}(r)$ via a linear combination of Gaussians. Alternatively, we can construct an approximation via a linear combination of Gaussians using (30).

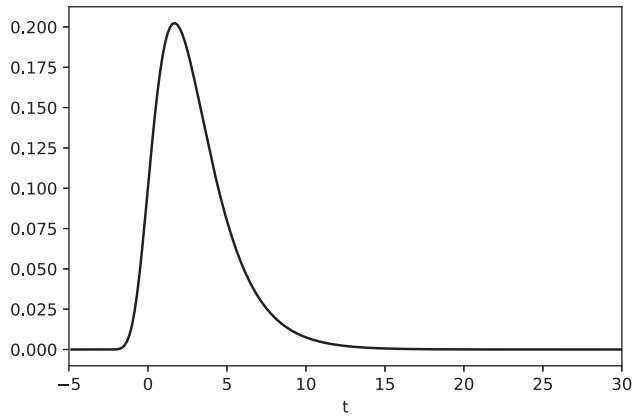

Fig. 1. Weight $w(t, 1)$ in the integral representation of $\overline{T}(p)$ in (28).

2.2.1. Spatial singularity of $\overline{T}$

To ascertain the behavior of $\overline{T}(r)$ near the singularity, we consider the weight function in (30) as the parameter $t \to \infty$. Evaluating contributions from the two terms in (30), we observe that

$$\frac{a}{\sqrt{2\pi}}\int_{-\infty}^{\infty} e^{-\frac{1}{4}e^t r^2} e^{-a^2 e^{-t}+t} dt = 2\sqrt{\frac{2}{\pi}}\frac{a^2}{r}K_1(ar) \sim 2a\sqrt{\frac{2}{\pi}}\frac{1}{r^2}. \tag{38}$$

Since $\mathrm{erfc}(ae^{-t/2}) \to 1$ as $t \to \infty$, for the second term in (30), we have

$$\frac{-a^2}{\sqrt{2}}\int_{-\infty}^{\infty} e^{-\frac{1}{4}e^t r^2} e^{\frac{1}{2}t} dt = \frac{-a^2\sqrt{\pi}}{\sqrt{2}\,r}, \tag{39}$$

a weaker singularity at $\|\mathbf{x}\| = 0$. This is expected since

$$\overline{T}(p) \sim \frac{2a}{p} - \frac{2a^2}{p^2} + O(p^{-3}) \tag{40}$$

for large p.

2.3. Representation of operator $\overline{E}$

Theorem 2. *Operator $\overline{E}$ with $\epsilon < 0$, has an integral representation*

$$\overline{E}(p, \epsilon) = \int_{-\infty}^{\infty} e^{-e^{-t}p^2} w(t, a, \epsilon) dt, \tag{41}$$

with the weight

$$w(t, a, \epsilon) = \frac{1}{c\sqrt{\pi}} e^{-\frac{1}{2}t} e^{-a^2 e^{-t}} \tag{42}$$

$$-(a/c + \epsilon/c^2) e^{-(a^2-(a+\epsilon/c)^2)e^{-t}-t} (\mathrm{erfc}((a+\epsilon/c)e^{-t/2}) - 2)$$

where $w(t-\tau, a, \epsilon) = e^{\frac{1}{2}\tau} w\left(t, ae^{\frac{1}{2}\tau}, \epsilon\, e^{\frac{1}{2}\tau}\right)$ and $a = mc$. *Spatial representation of $\overline{E}$ is then*

$$\overline{E}(r, \epsilon) = \int_{-\infty}^{\infty} e^{-\frac{1}{4}e^t r^2} \widetilde{w}(t, a, \epsilon) dt, \tag{43}$$

with the weight

$$\begin{aligned}\widetilde{w}(t, a, \epsilon) &= \frac{\pi}{c} e^t e^{-a^2 e^{-t}} - \pi^{3/2}(a/c + \epsilon/c^2) e^{-(a^2-(a+\epsilon/c)^2)e^{-t}+\frac{1}{2}t} \\ &\quad \left(\mathrm{erfc}\left((a+\epsilon/c)e^{-\frac{1}{2}t}\right) - 2\right).\end{aligned} \tag{44}$$

Proof. We have

$$\overline{E}(p, \epsilon) = (\sqrt{p^2c^2 + m^2c^4} - mc^2 - \epsilon)^{-1} = c^{-1}(\sqrt{p^2 + a^2} - a - \epsilon/c)^{-1} \tag{45}$$

and since

$$\frac{1}{\sqrt{p^2 + a^2} - a - \epsilon/c} - \frac{1}{\sqrt{p^2 + a^2} + a + \epsilon/c} = \frac{2(a + \epsilon/c)}{p^2 + a^2 - (a + \epsilon/c)^2} \tag{46}$$

obtain

$$\frac{1}{\sqrt{p^2 + a^2} - a - \epsilon/c} = \frac{1}{\sqrt{p^2 + a^2} + a + \epsilon/c} + \frac{2(a + \epsilon/c)}{p^2 + a^2 - (a + \epsilon/c)^2}. \tag{47}$$

Using

$$\frac{1}{\sqrt{p^2 + a^2} + a + \epsilon/c} = \int_0^{\infty} e^{-s(\sqrt{p^2+a^2}+a+\epsilon/c)} ds \tag{48}$$

and (33) to represent the first term in (47), we arrive at

$$\begin{aligned}&\frac{1}{\sqrt{p^2 + a^2} + a + \epsilon/c} \\ &= \int_{-\infty}^{\infty}\left(\int_0^{\infty} \frac{s}{2\sqrt{\pi}} e^{-s^2 e^t/4} e^{-s(a+\epsilon/c)} ds\right) e^{-(p^2+a^2)e^{-t}+\frac{1}{2}t} dt.\end{aligned} \tag{49}$$

Since

$$\begin{aligned}&\int_0^{\infty} \frac{s}{2\sqrt{\pi}} e^{-s^2 e^t/4} e^{-(a+\epsilon/c)s} ds \\ &= \frac{1}{\sqrt{\pi}} e^{-t} - (a + \epsilon/c) e^{(a+\epsilon/c)^2 e^{-t} - \frac{3}{2}t} \mathrm{erfc}((a + \epsilon/c)e^{-t/2}),\end{aligned} \tag{50}$$

we obtain

$$\frac{1}{\sqrt{p^2 + a^2} + a + \epsilon/c} = \int_{-\infty}^{\infty} e^{-p^2 e^{-t}} w_1(t, a, \epsilon) dt, \tag{51}$$

where

$$\begin{aligned}&w_1\left(t, a, \epsilon\right) \\ &= \frac{1}{\sqrt{\pi}} e^{-\frac{1}{2}t} e^{-a^2 e^{-t}} - (a + \epsilon/c) e^{(2a\epsilon/c + \epsilon^2/c^2)e^{-t} - t} \mathrm{erfc}((a + \epsilon/c)e^{-t/2}).\end{aligned} \tag{52}$$

For the second term in (47), we have

$$\begin{aligned}\tfrac{2(a+\epsilon/c)}{p^2+a^2-(a+\epsilon/c)^2} &= 2(a + \epsilon/c)\int_0^{\infty} e^{-s(p^2+a^2-(a+\epsilon/c)^2)} ds \\ &= 2(a + \epsilon/c)\int_{-\infty}^{\infty} e^{-e^{-t}(p^2+a^2-(a+\epsilon/c)^2)-t} dt \\ &= \int_{-\infty}^{\infty} e^{-e^{-t}p^2} w_2(t, a, \epsilon) dt,\end{aligned} \tag{53}$$

where

$$w_2(t, a, \epsilon) = 2(a + \epsilon/c) e^{-e^{-t}(a^2-(a+\epsilon/c)^2)-t}. \tag{54}$$

Combining (51) and (53) with weights (52) and (54), we arrive at (41) and (42). The scaling property of the weight is verified directly:

$$\begin{aligned}e^{\frac{1}{2}\tau} w\left(t, ae^{\frac{1}{2}\tau}, \epsilon\, e^{\frac{1}{2}\tau}\right) &= \tfrac{1}{c\sqrt{\pi}} e^{\frac{1}{2}\tau} e^{-\frac{1}{2}(t-\tau)} e^{-a^2 e^{\tau} e^{-t}} \\ &\quad -\left(ae^{\frac{1}{2}\tau}/c + \epsilon\, e^{\frac{1}{2}\tau}/c^2\right) e^{\frac{1}{2}\tau} e^{-\left(a^2 e^{\tau} - \left(ae^{\frac{1}{2}\tau} + \epsilon e^{\frac{1}{2}\tau}/c\right)^2\right) e^{-t} - t} \\ &\quad \left(\mathrm{erfc}\left(\left(ae^{\frac{1}{2}\tau} + \epsilon\, e^{\frac{1}{2}\tau}/c\right) e^{-t/2}\right) - 2\right) \\ &= w(t - \tau, a, \epsilon).\end{aligned} \tag{55}$$

On taking the Fourier transform in (41), we obtain (43).

2.3.1. Spatial singularity of $\overline{E}$

We consider the weight function in (44) as the parameter $t \to \infty$ and obtain

$$\widetilde{w}(t,a,\epsilon)\sim\frac{\pi}{c}e^{t}+2\pi^{3/2}(a/c+\epsilon/c^2)e^{\frac{1}{2}t}-\pi^{3/2}(a/c+\epsilon/c^2)\mathrm{erfc}(a+\epsilon/c) \tag{56}$$

and

$$\overline{E}(r,\epsilon)\sim\frac{\pi}{c}\int_{-\infty}^{\infty}e^{-\frac{1}{4}e^{t}r^2+t}dt+2\pi^{3/2}(a/c+\epsilon/c^2)\int_{-\infty}^{\infty}e^{-\frac{1}{4}e^{t}r^2+\frac{1}{2}t}dt. \tag{57}$$

As a result, the behavior of the kernel near the spatial singularity is estimated as

$$\overline{E}(r,\epsilon)\sim\frac{4\pi}{c}\frac{1}{r^2}+8\pi(a/c+\epsilon/c^2)\frac{1}{r}. \tag{58}$$

2.4. Representation of operator A

Theorem 3. *Operator A has an integral representation*

$$A(p)=\frac{1}{\sqrt{2}}+\frac{1}{\sqrt{2}}\int_{-\infty}^{\infty}e^{-\frac{p^2}{(mc)^2}e^{-t}}w_0(t)dt, \tag{59}$$

with the weight

$$w_0(t)=e^{-e^{-t}}\sum_{j=1}^{\infty}\frac{\sqrt{\pi}}{2\Gamma(j/2)\Gamma\left(\frac{1}{2}-j+1\right)j!}e^{-\frac{j}{2}t}, \tag{60}$$

where Γ is the gamma function. Spatial representation of A is then

$$A(r)=\frac{(2\pi)^{3/2}}{\sqrt{2}}\delta(\mathbf{x})+\widetilde{A}(r), \tag{61}$$

where the first term is (up to a factor) the identity operator and for the second term we have

$$\begin{aligned}\widetilde{A}(r)=&\frac{a^3}{4}\sum_{j=1}^{\infty}\frac{\alpha_j}{\Gamma(j/2)}\int_{-\infty}^{\infty}e^{-\frac{1}{4}a^2r^2e^{t}-e^{-t}+\frac{3-j}{2}t}dt\\ =&a^3\sum_{j=1}^{\infty}\frac{\alpha_j}{\Gamma(j/2)}2^{(1-j)/2}\left(\frac{1}{ar}\right)^{(3-j)/2}\mathrm{K}_{(3-j)/2}(ar)\\ =&a^3\left(\frac{1}{2\sqrt{\pi}}\frac{K_1(ar)}{ar}-\frac{\sqrt{2}}{16}\frac{K_{1/2}(ar)}{(ar)^{1/2}}+\frac{1}{16\sqrt{\pi}}K_0(ar)+\ldots\right),\end{aligned} \tag{62}$$

where $a=mc$. □

Proof. We have

$$A(p)=\frac{1}{\sqrt{2}}\sqrt{1+\frac{a}{\sqrt{r^2+a^2}}}, \tag{63}$$

where $a=mc$. We note that for $\|\mathbf{p}\|\neq 0$,

$$u=\frac{a}{\sqrt{r^2+a^2}}=\frac{1}{\sqrt{\frac{r^2}{a^2}+1}}<1 \tag{64}$$

so that

$$\sqrt{1+u}=1+\sum_{j=1}^{\infty}\alpha_j u^j, \tag{65}$$

where

$$\alpha_j=\frac{\sqrt{\pi}}{2\Gamma\left(\frac{1}{2}-j+1\right)j!}. \tag{66}$$

We have

$$A(p)=\frac{1}{\sqrt{2}}+\frac{1}{\sqrt{2}}\sum_{j=1}^{\infty}\alpha_j\frac{1}{\left(\sqrt{\frac{p^2}{a^2}+1}\right)^j}, \tag{67}$$

apply (22) with $\alpha=j$ and arrive at

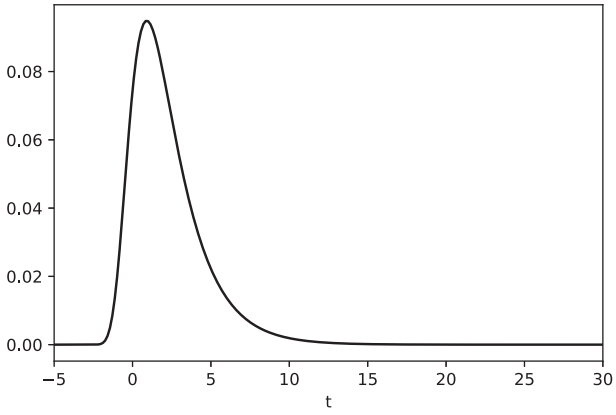

Fig. 2. Weight $w_0(t)$ in the integral representation of $A(p)$ in (60).

$$A(p)=\frac{1}{\sqrt{2}}+\frac{1}{\sqrt{2}}\sum_{j=1}^{\infty}\frac{\alpha_j}{\Gamma(j/2)}\int_{-\infty}^{\infty}e^{-\left(\frac{p^2}{a^2}+1\right)e^{-t}-\frac{j}{2}t}dt \tag{68}$$

and the result. On taking the Fourier transform we arrive at the spatial representation of $A(p)$ (61) and (62). The weight in (60) is illustrated in Fig. 2.

2.4.1. Spatial singularity of A

Using (62), we obtain that

$$\widetilde{A}(r)\sim C_2\frac{1}{r^2} \tag{69}$$

near the singularity, where C_2 is a constant. Again, this is expected since

$$A(p)\sim\frac{1}{\sqrt{2}}+\frac{a}{2\sqrt{2}p}+O(p^{-2}). \tag{70}$$

2.5. Representation of operator $\overline{P}A$

Theorem 4. *Operator $\overline{P}A$ has an integral representation*

$$\overline{P}(p)A(p)=\int_{-\infty}^{\infty}e^{-\frac{p^2}{a^2}e^{-t}}w(t)dt, \tag{71}$$

with the weight

$$w(t)=\frac{1}{a\sqrt{2}}e^{-e^{-t}-\frac{1}{2}t}\sum_{j=0}^{\infty}\frac{\widetilde{\alpha}_j}{\Gamma\left(\frac{j+1}{2}\right)}e^{-\frac{j}{2}t}, \tag{72}$$

where Γ is the gamma function and

$$\widetilde{\alpha}_j=\frac{\sqrt{\pi}}{\Gamma\left(\frac{1}{2}-j\right)j!}. \tag{73}$$

Spatial representation of $\overline{P}A$ is then

$$\overline{P}A(r)=\int_{-\infty}^{\infty}e^{-\frac{1}{4}e^{t}a^2r^2}\widetilde{w}(t)dt \tag{74}$$

$$=a^2\left(\frac{1}{\sqrt{\pi}ar}\mathrm{K}_1(ar)-\frac{1}{2\sqrt{2}}\left(\frac{1}{ar}\right)^{1/2}\mathrm{K}_{1/2}(ar)+\ldots\right), \tag{75}$$

where

$$\widetilde{w}(t)=\frac{a^2}{4}e^{-e^{-t}+t}\sum_{j=0}^{\infty}\frac{\widetilde{\alpha}_j}{\Gamma\left(\frac{j+1}{2}\right)}e^{-\frac{j}{2}t}. \tag{76}$$

Proof. We have

$$\overline{P}(p)A(p) = \frac{1}{\sqrt{2}}(p^2 + a^2)^{-1/2}\left(1 + \frac{a}{\sqrt{p^2 + a^2}}\right)^{-1/2} = \frac{1}{a\sqrt{2}}u(1+u)^{-1/2}, \tag{77}$$

where $a = mc$ and

$$u = \frac{a}{\sqrt{p^2 + a^2}} = \frac{1}{\sqrt{\frac{p^2}{a^2} + 1}} \leq 1. \tag{78}$$

Expanding into series at $u = 0$,

$$(1+u)^{-1/2} = \sum_{j=0}^{\infty} \widetilde{\alpha}_j u^j, \tag{79}$$

where

$$\widetilde{\alpha}_j = \frac{\sqrt{\pi}}{\Gamma\left(\frac{1}{2} - j\right)j!}, \tag{80}$$

we obtain

$$\overline{P}(p)A(p) = \frac{1}{a\sqrt{2}}\sum_{j=0}^{\infty}\widetilde{\alpha}_j\left(\frac{1}{\sqrt{\frac{p^2}{a^2}+1}}\right)^{j+1}. \tag{81}$$

Next, applying (22) with $\alpha = j+1$, we arrive at

$$\overline{P}(p)A(p) = \frac{1}{a\sqrt{2}}\sum_{j=0}^{\infty}\frac{\widetilde{\alpha}_j}{\Gamma\left(\frac{j+1}{2}\right)}\int_{-\infty}^{\infty} e^{-\left(\frac{p^2}{a^2}+1\right)e^{-t} - \left(\frac{j}{2}+\frac{1}{2}\right)t}dt \tag{82}$$

yielding the representation. In the real space we have

$$\frac{1}{(2\pi)^{3/2}}\int_{\mathbb{R}^3} e^{-\frac{\mathbf{p}^2}{a^2}e^{-t}}e^{i\mathbf{rp}}d\mathbf{p} = \frac{a^3}{2^{3/2}}e^{-\frac{1}{4}e^t a^2 r^2 + \frac{3}{2}t} \tag{83}$$

and obtain the weight (76) We can rewrite (74) using the Bessel functions,

$$\begin{aligned}\overline{P}A(r) &= \frac{a^2}{4}\int_{-\infty}^{\infty} e^{-\frac{1}{4}e^t a^2 r^2}e^{-e^{-t}}\sum_{j=0}^{\infty}\frac{\widetilde{\alpha}_j}{\Gamma\left(\frac{j+1}{2}\right)}e^{\frac{(2-j)}{2}t}dt \\ &= \frac{a^2}{4}\sum_{j=0}^{\infty}\frac{\widetilde{\alpha}_j}{\Gamma\left(\frac{j+1}{2}\right)}\int_{-\infty}^{\infty} e^{-\frac{1}{4}e^t a^2 r^2}e^{-e^{-t}}e^{\frac{(2-j)}{2}t}dt \\ &= a^2\sum_{j=0}^{\infty}\frac{\widetilde{\alpha}_j}{2^{j/2}\Gamma\left(\frac{j+1}{2}\right)}\left(\frac{1}{ar}\right)^{(2-j)/2}\mathrm{K}_{(2-j)/2}(ar),\end{aligned} \tag{84}$$

so that we have (75). □

2.5.1. Spatial singularity of $\overline{P}A$

We note that the weight of the second term in (74) simplifies as $t \to \infty$ and we have the integral

$$\overline{P}A(r) \sim C_1\int_{-\infty}^{\infty} e^{-\frac{1}{4}a^2r^2e^t}e^{-e^{-t}+t}dt \sim C_2\frac{1}{r^2}, \tag{85}$$

where C_1 and C_2 are constants. This is expected since

$$\overline{P}A(p) \sim \frac{1}{\sqrt{2}p} + O(p^{-2}). \tag{86}$$

2.6. Efficient accommodation of fine scales

The operators with kernels that behave as $O(r^{-2})$ near the origin in real space (due to the slow asymptotic decay as p^{-1} in Fourier space) require a significantly larger number of fine length scales in their representation than operators behaving as $O(r^{-1})$ near the origin. As an example, let us consider the radial kernel $r^{-\alpha}$, $0 < \alpha < d$, where $r = \sqrt{\sum_{l=1}^{d} x_l^2}$ and dimension $d = 3$ is of immediate interest. We consider applying this operator to compactly supported functions which, for simplicity, are rescaled to have support inside the box $D = [-1/2\sqrt{2}, 1/2\sqrt{2}]^d$. For $\mathbf{x} \in D$, we want to compute

$$\begin{aligned}(Tf)(\mathbf{x}) &= \int_{\mathbb{R}^d}\left\|\mathbf{z}-\mathbf{x}\right\|^{-\alpha}f(\mathbf{z})d\mathbf{z} = \int_{\mathbb{R}^d}\left\|\mathbf{y}\right\|^{-\alpha}f\left(\mathbf{x}+\mathbf{y}\right)d\mathbf{y} \\ &= \int_{B_1}\left\|\mathbf{y}\right\|^{-\alpha}f\left(\mathbf{x}+\mathbf{y}\right)d\mathbf{y},\end{aligned} \tag{87}$$

where B_r denotes the ball of radius r centered at $\mathbf{y} = \mathbf{0}$. We replace the kernel by its approximation via Gaussians constructed to be accurate in the interval $\delta \leqslant r \leq 1$,

$$G_F(r) = G_F\left(r;M,N,h\right) = \frac{h}{\Gamma(\alpha/2)}\sum_{n=M+1}^{N} e^{h\alpha n/2}e^{-e^{hn}r^2}, \tag{88}$$

and estimate the resulting error. At issue is the impact of approximation (88) in the region $0 \leqslant r < \delta$, which in contrast with the kernel, has no singularity at $r = 0$. The following estimate is demonstrated in [18, Theorem 12].

Theorem 5. *Let* $0 < \alpha < d$ *and*

$$|r^{-\alpha} - G_F(r)| \leqslant \epsilon\, r^{-\alpha} \tag{89}$$

be an approximation of the kernel by Gaussians valid for $\delta \leqslant r \leq 1$. *Then, for any bounded, compactly supported function* f *in* D *and* $x \in D$, *we have*

$$\left|\int_{B_1}\left\|\mathbf{y}\right\|^{-\alpha}f\left(\mathbf{x}+\mathbf{y}\right)d\mathbf{y} - \int_{B_1}G_F\left(\left\|y\right\|\right)f\left(\mathbf{x}+\mathbf{y}\right)d\mathbf{y}\right| \leqslant (\epsilon + (2+\epsilon)\delta^{d-\alpha})\frac{\omega_{d-1}}{d-\alpha}\left\|f\right\|_{\infty}, \tag{90}$$

where $\omega_{d-1} = 2\pi^{d/2}/\Gamma(d/2)$ *is the surface area of the unit sphere in* $\mathbb{R}^d$.

This estimate shows that for operators whose kernels behave as $O(r^{-2})$ near the origin $\delta \sim \epsilon$, whereas for kernels behaving near the origin as $O(r^{-1})$ $\delta \sim \sqrt{\epsilon}$. This is why we need expansions that are accurate to very high momenta corresponding to small length scales that are otherwise not physically relevant. However, application of these expansions can be simplified to reduce their contribution to the overall computational cost.

Consider convolving a Gaussian $g(\tau, \mathbf{x}) = \left(\frac{\tau}{\pi}\right)^{3/2}\exp(-\tau x^2)$ with a large exponent τ with some function $f(\mathbf{x})$ that on the length scale of the Gaussian is smooth. We have $\int_{\mathbb{R}^3} g(\tau, \mathbf{x})d\mathbf{x} = 1$ and

$$\begin{aligned}(g * f)(\mathbf{x}) &= \int_{\mathbb{R}^3} g(\tau, \|\mathbf{y}\|)f(\mathbf{x}-\mathbf{y})d\mathbf{y} \\ &= f(\mathbf{x}) + \frac{1}{2}\sum_{i=1}^{3}\frac{\partial^2 f(\mathbf{x})}{\partial^2 x_i}\int_{\mathbb{R}^3} g(\tau, \|\mathbf{y}\|)y_i^2 d\mathbf{y} + \ldots\end{aligned} \tag{91}$$

The first term in the error can be bounded

$$\begin{aligned}\left|\frac{1}{2}\sum_{i=1}^{3}\frac{\partial^2 f(\mathbf{x})}{\partial^2 x_i}\int_{\mathbb{R}^3} g(\tau, \|\mathbf{y}\|)y_i^2 d\mathbf{y}\right| &\leqslant \frac{1}{2}\sum_{i=1}^{3}\left|\frac{\partial^2 f(\mathbf{x})}{\partial^2 x_i}\right|\int_{\mathbb{R}^3} g(\tau, \|\mathbf{y}\|)y_i^2 d\mathbf{y} \\ &= \frac{1}{4\tau}\sum_{i=1}^{3}\left|\frac{\partial^2 f(\mathbf{x})}{\partial^2 x_i}\right| \\ &\leqslant \frac{3}{4\tau}\max_{i=1,2,3}\left|\frac{\partial^2 f(\mathbf{x})}{\partial^2 x_i}\right|\end{aligned} \tag{92}$$

and the subsequent terms are $O(\tau^{-2})$.

Given representation of the kernel via Gaussians $g(\tau_j, \mathbf{x})$, e.g. (88), we select a sufficiently large $\tau = \tau_{max}$ and all Gaussian terms with the exponent $\tau \geqslant \tau_{max}$ are replaced by the identity operator scaled by the sum of the coefficients of these terms. In the context of relativistic electronic structure calculations employing a Gaussian atomic basis set the largest exponent in the operator (τ_{max}) could be chosen to be somewhat larger than the largest exponent in the atomic basis. Similarly, if employing a finite nucleus model or with a numerical grid with

a finite resolution then either the physics or numerics define a finest length scale (δx) and we can pick $\tau_{max} \gg \delta x^{-2}$. If the basis is capable of representing the singular form of the (quasi-) relativistic wave functions then it is still feasible to employ an untruncated real-space operator since the number of terms only grows logarithmically with either the desired accuracy or finest length scale.

Finally, instead of handling the identity operator explicitly (by adding the appropriate multiple of the input function to the result), we instead combine all coefficients of terms with $\tau \geqslant \tau_{max}$ as the coefficient of the Gaussian with largest exponent τ_{max}. The benefits of this are making application of these operators consistent with other operators, and thus incorporating into the operator a filter with a bandlimit implied by the choice of finest length scale. This latter characteristic is of specific benefit in controlling high-frequencies when computing with near singular solutions in the discontinuous multiwavelet basis. Consideration of the coefficients of the normalized Gaussians also enables pruning terms with small norm-wise contribution, though this was not done in any of the numerical tests below.

2.7. Outline of DKH2 approach

In the second-order case, we must in addition represent W_1 (Eq. (13)). Obtaining its separated representation is simplified if we represent the denominator using (23) as

$$\frac{1}{E_0(\mathbf{p}) + E_0(\mathbf{p}')} = \int_{-\infty}^{\infty} \exp(-(E_o(\mathbf{p}) + E_0(\mathbf{p}'))\exp(-t) - t)dt, \tag{93}$$

which can be approximated via numerical quadrature to maintain

$$\left| \frac{1}{E_0(\mathbf{p}) + E_0(\mathbf{p}')} - \sum_{m=1}^{M} e^{-t_m} e^{-e^{-t_m} E_0(\mathbf{p})} e^{-e^{-t_m} E_0(\mathbf{p}')} \right| \leqslant \epsilon \tag{94}$$

leading to

$$\left| W(\mathbf{p}, \mathbf{p}') - \sum_{m=1}^{M} e^{-t_m} e^{-e^{-t_m} E_0(\mathbf{p})} A(p)(P(\mathbf{p}) - P(\mathbf{p}'))A(p') e^{-e^{-t_m} E_0(\mathbf{p}')} V_{ext}(\mathbf{p} - \mathbf{p}') \right| \leqslant \frac{C\epsilon}{\|\mathbf{p} - \mathbf{p}'\|}. \tag{95}$$

While accurate with the techniques outlined above, applying $W_1 O_1 + O_1 W_1$ using the above formulation requires $24M$ operator applications, where M is the number of quadrature points, even when accounting for commutativity of operators where possible. This is impractically expensive in the intended context of computation with the multiwavelet basis, and therefore is not explored further here.

3. Demonstration and discussion

3.1. Real-space form of the operators

Using the expansions, it is possible for the first time to see the kernel of each operator plotted in real space as shown in Fig. 3. Near the origin, all operators exhibit the anticipated $O(r^{-2})$ singularity and at long range (i.e. $r \gg c^{-1}$) exhibit exponential decay.

In Fig. 4, we plot both $\overline{E}$ and its long-range asymptotic form, which is the nonrelativistic Green's function $g(r, \varepsilon) = e^{-\sqrt{-2\varepsilon}r}/(4\pi r)$. For both $\overline{E}$ and g, the parameter ϵ is taken to be -0.5000066566, the analytic ground state energy for the Dirac hydrogen atom. It is again apparent that the asymptotic form starts to dominate for $r \gg c^{-1}$.

3.2. Accuracy demonstration

Given the desired range of validity of each operator, three parameters must be chosen to construct each expansion in real space: the upper and lower bounds of the quadrature points used in the approximation of the integrals over t, and the number of quadrature points to be used. For the calculations below, each of the operators was integrated from $t = -5$ to $t = 105$, using 450 points. These values were chosen to converge the value of each operator to the 16th significant digit from $r = 10^{-16}$ to where the operators become exponentially small in real space, where we maintain an absolute error of $O(10^{-16})$. Lower accuracy, but more compact, representations can be obtained by reducing the number of quadrature points. Infinite sums present in A and $\overline{P}A$ were evaluated by turning them into finite sums via an approximation with exponentials as described in Section 2, using methods presented in [17,18], but similar results can be achieved using a Padè summation technique to approximate the infinite sums.

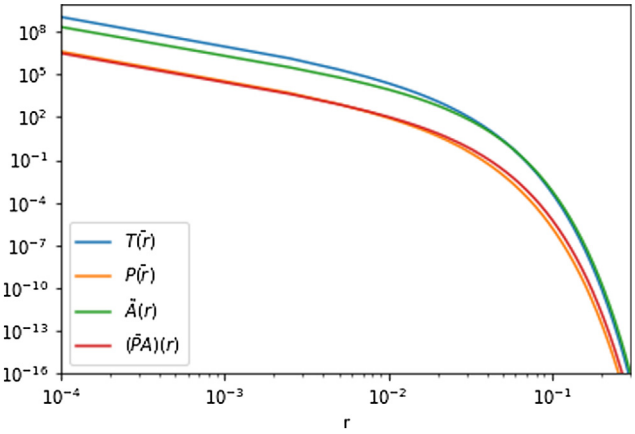

Fig. 3. Real-space plot of the operators required for first-order Douglas-Kroll-Hess theory. All operators have $O(r^{-2})$ singularities at the origin and decay exponentially past approximately $1/c$, which can be understood from looking at their Fourier-space representations.

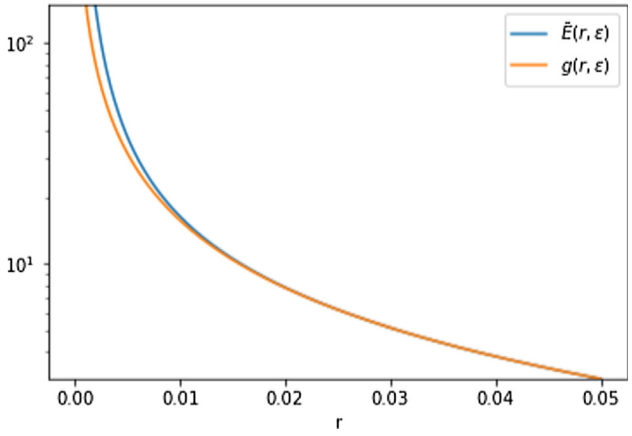

Fig. 4. Real-space plot of the operator $\overline{E}$, and its non-relativistic counterpart, the bound-state Helmholtz Green's function. $\epsilon = -0.5000066566$. $\overline{E}$ also has an $O(r^{-2})$ singularity at the origin, and at long distance coincides with the non-relativistic Green's function.

Since the analytic form of the operators in real space is not known, there is no straightforward comparison that can be made to verify the accuracy of the real-space expansions presented in Section 2. It is for this reason that we present three indirect accuracy checks. As an initial check for accuracy, each expansion was integrated over all 3D space. For each, the result matches the analytic value, evaluated using the momentum-space representation at the origin, to a relative accuracy of $O(10^{-17})$. Second, for each operator, we verified the leading coefficient in its asymptotic expansion, and in each case the result matched that shown in Section 2 to a relative error of $O(10^{-15})$. Finally, we take the Fourier transform of the real-space expansions, and compare these with the known momentum-space analytic forms. As an example, below are plots of the absolute and relative error for $\overline{P}$ (see Fig. 5).

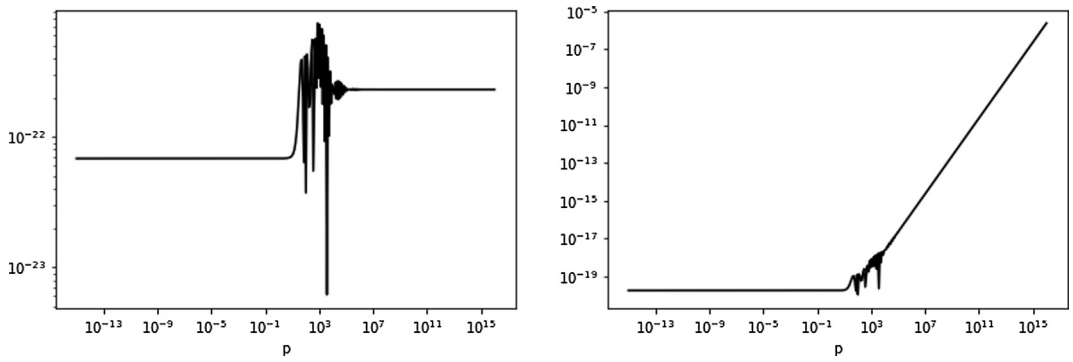

Fig. 5. Left: Plot of the absolute error in the Fourier-transformed Gaussian expansion for $\overline{P}$. Both axes are log scale. Right: Plot of the relative error in the Fourier-transformed Gaussian expansion for $\overline{P}$. Both axes are log scale.

Table 1
RK ground state energy results for a selection of hydrogen-like systems, in units of Hartree.

Z	Gaussian Basis	MRA Basis
1	−0.5000329700269	−0.500032934
2	−2.00052296210	−2.0005228
4	−8.00823785074	−8.0082375
8	−32.1284787490	−32.128476
16	−129.987729629	−129.98772
20	−204.806968723	−204.80696
32	−543.410198039	−543.41015
40	−878.142019649	−878.14195
48	−1320.11622098	−1320.1161
56	−1898.13981088	−1898.1396
60	−2252.40685821	−2252.4065
64	−2662.13109180	−2662.1306
72	−3712.08905456	−3712.0861
76	−4412.04702772	−4412.0262
80	−5317.78764638	−5317.5395

Table 2
DKH1 ground state energy results for a selection of hydrogen-like systems, in units of Hartree. Comparison is made to reference [24] where available.

Z	Gaussian Basis	MRA Basis	Literature [24]
1	−0.500006809339	−0.50000683	
2	−2.00011113727	−2.0001112	
4	−8.00183970323	−8.0018401	
8	−32.0310364850	−32.031037	
16	−128.534391137	−128.53438	
20	−201.341496401	−201.34149	−201.34149611
32	−521.406611413	−521.40659	
40	−823.894232024	−823.89419	−823.89422633
48	−1203.54710246	−1203.5470	
56	−1667.58039393	−1667.5802	
60	−1934.20286732	−1934.2027	−1934.202797
64	−2225.90140509	−2225.9012	
72	−2892.28889021	−2892.2886	
76	−3271.84799672	−3271.8477	
80	−3686.44880964	−3686.4484	−3686.44746

3.3. Application

Finally, the expansions were tested for various hydrogen-like systems using both the RK and DKH1 Hamiltonians, in both the multiresolution basis and an even-tempered Gaussian basis set. Results are shown in Tables 1 and 2.The Gaussian basis sets used 200 even-tempered exponents ranging from $Z^2 \cdot 10^{-3}$ to $Z^2 \cdot 10^{25}$, where Z is the charge of the point nucleus. Numerical results suggest that the results using the Gaussian basis are converged to all digits presented. For the multiresolution calculations, the user must set the number of mother scaling functions used to construct the basis as well as the desired refinement threshold[22]. For these parameters we used 10 and 10^{-8}, respectively. All calculations use the value $c = 137.0359895$ [23] for consistency when comparing with literature [24].

4. Conclusions

For the first time, real-space, arbitrarily-accurate representations for first- and second-order Douglas-Kroll-Hess operators have been presented. Each representation is written as a sum of Gaussian functions with positive coefficients, and we note that this approach should be applicable to other operator-based quasi-relativistic models. The real-space construction allows for application of these operators to real-space functions, such as atom-centered Gaussians or multiwavelets, circumventing the need to compute using approximate eigenfunctions of p^2. The use was demonstrated in ground-state calculations of hydrogen-like systems using the relativistic-kinematic and first-order DKH Hamiltonians. Extension of this method to higher order terms leads to prohibitively expensive calculations in the multiwavelet basis due to the high number of operator applications, but in a basis of atom-centered Gaussians such an extension this should be tractable due to the analytic evaluation of the integrals involved.

Declaration of Competing Interest

The authors declare that they have no known competing financial interests or personal relationships that could have appeared to influence the work reported in this paper.

Acknowledgement

Anderson, Harrison, Sundahl, and Thornton were supported in part by the NSF under grant ACI-1450344.

References

[1] P. Pyykkö, Relativistic effects in structural chemistry, Chem. Rev. 88 (1988) 563–594.
[2] M. Douglas, N. Kroll, Quantum electrodynamical corrections to the fine structure of Helium, Ann. Phys. 82 (1974) 89–155.
[3] M. Barysz, A.J. Sadlej, Infinite-order two-component theory for relativistic quantum chemistry, J. Chem. Phys. 116 (7) (2002) 2696–2704.
[4] A. Wolf, M. Reiher, B.A. Hess, The generalized Douglas-Kroll transformation, J. Chem. Phys. 117 (20) (2002) 9215–9226.
[5] W.L.W. Kutzelnigg, Quasirelativistic theory equivalent to fully relativistic theory, J. Chem. Phys. 123 (2005) 241102.
[6] R. Harrison, G. Fann, T. Yanai, Z. Gan, G. Beylkin, Multiresolution quantum chemistry: basic theory and initial applications, J. Chem. Phys. 121 (23) (2004) 11587–11598.
[7] B. Hess, Relativistic electronic-structure calculations employing a no-pair formalism with external-field projection operators, Phys. Rev. A 33 (6) (1986) 3742–3748.
[8] W. Liu, Ideas of relavistic quantum chemistry, Mol. Phys. 108 (13) (2010) 1679–1706.
[9] T. Saue, Relativistic Hamiltonians for chemistry: a primer, ChemPhysChem 12 (2011) 3077–3094.

[10] M. Reiher, Relativistic Douglas-Kroll-Hess theory, Wiley Interdiscip. Rev.: Comput. Mol. Sci. 2 (2012) 139–149.
[11] K.G. Dyall, An exact separation of the spin-free and spin-dependent terms of the Dirac-Coulomb-Breit Hamiltonian, J. Chem. Phys. 100 (3) (1994) 2118–2127.
[12] K.G. Dyall, Interfacing relativistic and nonrelativistic methods. I. Normalized elimination of the small component in the modified Dirac equation, J. Chem. Phys. 106 (23) (1997) 9618–9626.
[13] L. Foldy, S. Wouthuysen, On the Dirac theory of spin 1/2 particles and its non-relativistic limit, Phys. Rev. 78 (1) (1950) 29–36.
[14] C. van Wullen, On the eigenfunctions of the Douglas-Kroll operator, Chem. Phys. 356 (2009) 199–204.
[15] B. Alpert, G. Beylkin, D. Gines, L. Vozovoi, Adaptive solution of partial differential equations in multiwavelet bases, J. Comput. Phys. 182 (1) (2002) 149–190.
[16] R. Harrison, G. Fann, T. Yanai, G. Beylkin, Multiresolution quantum chemistry in multiwavelet bases, in: P.M.A. Sloot, et al. (Ed.), Lecture Notes in Computer Science, Computational Science-ICCS 2003, vol. 2660, Springer, 2003, pp. 103–110.
[17] G. Beylkin, L. Monzón, On approximation of functions by exponential sums, Appl. Comput. Harmon. Anal. 19 (1) (2005) 17–48.
[18] G. Beylkin, L. Monzón, Approximation of functions by exponential sums revisited, Appl. Comput. Harmon. Anal. 28 (2) (2010) 131–149.
[19] G. Fann, J. Pei, R. Harrison, J. Jia, J. Hill, M. Ou, W. Nazarewicz, W. Shelton, N. Schunck, Fast multiresolution methods for density functional theory in nuclear physics, J. Phys.: Conf. Ser, vol. 180, IOP Publishing, 2009, p. 012080.
[20] L. Genovese, T. Deutsch, A. Neelov, S. Goedecker, G. Beylkin, Efficient solution of Poisson's equation with free boundary conditions, J. Chem. Phys. 125 (7) (2006).
[21] G. Beylkin, G. Fann, R.J. Harrison, C. Kurcz, L. Monzón, Multiresolution representation of operators with boundary conditions on simple domains, Appl. Comput. Harmon. Anal. 33 (2012) 109–139, https://doi.org/10.1016/j.acha.2011.10.001.
[22] R. Harrison, G. Fann, Z. Gan, T. Yanai, S. Sugiki, A. Beste, G. Beylkin, Multiresolution computational chemistry, J. Phys.: Conf. Ser, vol. 16, IOP Publishing, 2005, p. 243.
[23] L. Visscher, K. Dyall, Dirac-Fock atomic electronic structure calculations using different nuclear charge distributions, At. Data Nucl. Data Tables 67 (2) (1997) 207–224.
[24] A.W.M. Reiher, Exact decoupling of the Dirac Hamiltonian. II. The generalized Douglas-Kroll-Hess transformation up to arbitrary order, J. Chem. Phys. 121 (22) (2004) 10945–10956.